Follow us @BoneJointRes

Freely available online OPEN ACCESS

BJR

BIOMATERIALS

3D-printed titanium implant combined with interleukin 4 regulates ordered macrophage polarization to promote bone regeneration and angiogenesis

D-W. Zhao,
B. Ren,
H-W. Wang,
X. Zhang,
M-Z. Yu,
L. Cheng,
Y-H. Sang,
S-S. Cao,
F. M. Thieringer,
D. Zhang,
Y. Wan,
C. Liu

From Qilu Hospital, Shandong University, Jinan, China

Aims

The use of 3D-printed titanium implant (DT) can effectively guide bone regeneration. DT triggers a continuous host immune reaction, including macrophage type 1 polarization, that resists osseointegration. Interleukin 4 (IL4) is a specific cytokine modulating osteogenic capability that switches macrophage polarization type 1 to type 2, and this switch favours bone regeneration.

Methods

IL4 at concentrations of 0, 30, and 100 ng/ml was used at day 3 to create a biomimetic environment for bone marrow mesenchymal stromal cell (BMMSC) osteogenesis and macrophage polarization on the DT. The osteogenic and immune responses of BMMSCs and macrophages were evaluated respectively.

Results

DT plus 30 ng/ml of IL4 (DT + 30 IL4) from day 3 to day 7 significantly ($p < 0.01$) enhanced macrophage type 2 polarization and BMMSC osteogenesis compared with the other groups. Local injection of IL4 enhanced new bone formation surrounding the DT.

Conclusion

DT + 30 IL4 may switch macrophage polarization at the appropriate timepoints to promote bone regeneration.

Cite this article: *Bone Joint Res* 2021;10(7):411–424.

Keywords: Interleukin 4, 3D-printed titanium implant, macrophage polarization

Article focus

- Mechanisms of bone regeneration under macrophage conditioned culture system via different concentrations of interleukin 4 (IL4).
- Appropriate timepoint of IL4 delivery in vitro to maximize bone marrow mesenchymal stromal cell (BMMSC) osteogenesis.
- The differences of 3D-printed titanium implant (DT) and DT + 30 IL4 in osteo-immunomodulation and osteogenesis in vivo.

Key messages

- BMMSCs cultured on DT and DT+ IL4 have good cell viability and proliferation.
- Osteogenic and angiogenic markers were enhanced with 30 IL4 delivery from the third day to the seventh day in vitro.
- DT + 30 IL4 (from the third day to the seventh day) is an osteoimmunomodulatory biomaterial which can promote osteogenesis in vivo.

Strengths and limitations

- This study demonstrated the effect of DT + IL4 in promoting bone regeneration and angiogenesis via ordered macrophage polarization.
- This study introduced an accurate and proactive immunomodulatory strategy via 30 IL4 delivery from the third day to the seventh day.

Correspondence should be sent to Chao Liu; email: qiluliuchao@sdu.edu.cn

doi: 10.1302/2046-3758.107.BJR-2020-0334.R4

Bone Joint Res 2021;10(7):411–424.

- Further research is required to fully illustrate the mechanism of IL4 in M2 macrophage-mediated immune response.

Introduction

Bone tissue engineering is a vital strategy in bone regeneration; it relies on the development of materials and fabrication processes.[1] Titanium (Ti) plays a key role in several biomedical applications,[2] including bone grafting for injuries and tumour-induced bone defects. However, currently used Ti alloy plates are manufactured only in fixed arcuate shapes, and they require adjustment during surgery, which is time-consuming and may place patients at risk. Additive manufacturing and 3D printing offer a variety of solutions to the manufacturing problems associated with conventional techniques. One major problem associated with additive manufacturing is evolution of residual stresses, leading to deformed parts and formation of defects such as pores and cracks, all of which are detrimental to the quality of deposits.[3] During the fabrication of 3D-printed titanium implants (DTs), some Ti powder is not completely melted, thereby forming on the surface of the DT. Spherical powders with diameters of 50 μm have been detected on DTs, and this gives rise to rough surface topography.

Macrophages cultured on Ti surfaces exhibited a tendency to polarize to M1 phenotype with increased surface roughness (ranging approximately 100 nm to 400 nm).[4] In this manner, DT is likely to induce persistent M1 polarization after implantation. Continuous M1 polarization can clear foreign bodies in the early stages; however, inflammatory products in the mid-to-late stages are detrimental to osteogenesis. To assist DT in the regulation of osteoimmunomodulation, it would be important to administer an appropriate dose of an M2 agonist three days after implantation.

Following placement of the Ti implant, immune cells such as macrophages accumulate on its surface and trigger immune reactions.[5] The persistent inflammation caused by macrophage type 1 (M1) polarization produces fibrous encapsulation surrounding the Ti implants, and promotes bone destruction by inducing the activation of osteoclasts to suppress osteogenesis.[6] However, under physiological conditions, appropriate immune reactions caused by polarization to macrophage type 2 (M2) are beneficial for osseointegration.[7] Acute inflammation is thought to be the first stage of tissue healing;[8] M1 macrophages clear debris and bacterial pathogens at this stage.[9] Subsequently, the switch from M1 to M2 is delayed to three days post-implantation; this is the time when levels of inflammatory cytokines begin to decline during normal bone healing.[10,11] The switch between M1 and M2 has an impact on bone regeneration. For this reason, it is difficult to achieve the optimal bone-forming effect with a single regulatory factor on the DT scaffold. Controllable elements based on immunological characteristics are necessary. A study reported that silanized Ti possesses anti-inflammatory properties, and promotes M2 polarization with modest engagement of the nuclear factor-κB signalling pathway.[12] Ti nanotubes (produced by anodic oxidation) induced macrophage polarization toward the anti-inflammatory M2 state and increased the expression of arginase-1, mannose receptor, and interleukin 10 (IL10).[13] Nevertheless, these modifications of various Ti implants only produced constant induction of M2 polarization, and could not achieve dynamic regulation of M1 and M2.

Yang et al[14] reported that GG07-I (releasing IL4) prompted the switch from M1 to M2 phenotype. Genetically modified IL4-secreting mesenchymal stromal cells (MSCs) and preconditioned MSCs showed potential for optimizing bone regeneration under inflammatory conditions, including periprosthetic osteolysis.[15] Immobilization of IL4 using polydopamine is convenient and effective for controlling macrophage behaviour upon implant insertion, further accelerating bone integration.[16] IL4 drives the transition of macrophages to pro-healing M2 in vitro and in vivo,[11] and this has been linked to enhanced osteogenic and angiogenic properties of these materials. It has been reported that the delivery of IL4 significantly enhanced decellularized bone matrix-mediated osteogenesis and angiogenesis via the coordinated involvement of M1 and M2.[11] In fact, M1 and M2 play different roles in various stages of inflammation that are beneficial for osteogenesis. During the entire inflammatory process, M1 and M2 are both present in a dynamic balance, and the rational combination of DT and IL4 determines the balance of M1/M2, thereby achieving good osteogenesis and angiogenesis via accurate immunomodulation.

In this study, we proactively constructed and optimized an inflammatory microenvironment by delivering IL4, and we evaluated its potential for promoting DT-related osteogenesis and angiogenesis. To mimic the inflammation-related microenvironment of implants in vivo, we investigated the effects of IL4 concentrations and DT surface morphology on the osteoimmunomodulation of implants.

Methods

Scaffold preparation. DT sheets (10 mm × 10 mm × 1 mm) and cylinders (diameter 2 mm × 5 mm) designed for in vitro and in vivo experiments, respectively, were fabricated using a metal 3D printing machine (Q10 plus; Arcam, Sweden). Ti-6Al-4V alloy powder, with diameters ranging from 45 μm to 106 μm, was used as the raw material. The printing process, based on electron beam melting (EBM) technique, was performed following the guidelines provided by the manufacturer.

The detailed fabrication process was as follows. Prior to printing, the chamber was initially filled with helium (regulating gas) to minimize oxidation, and was heated to 750°C. Subsequently, a thin layer of Ti-6Al-4V powder (thickness: 50 μm) was spread over the printing bed, followed by electron beam scanning to melt the powder.

The powder feeding and scanning processes were performed in alternating fashion. In this manner, the final construct was produced layer-by-layer with a printing velocity of 800 mm·s^{-1}. The diameter of the electron beam is 100 μm and the mean power is 900 ± 40 W. Following completion of the printing process, the samples were detached from the printing bed and were ultrasonically cleaned in distilled water. High-pressure steam sterilization was performed for subsequent in vitro and in vivo experiments.

Surface characteristics. A field emission scanning electron microscope (JSM-7800F; JEOL, Japan) equipped with an energy dispersive X-spectroscope was used to observe the surface morphology and to determine the element composition of the DT.

Isolation, culture, and identification of bone marrow mesenchymal stromal cells. Femora from four-week-old male Sprague Dawley rats were dissected and the bone marrows were flushed using 18-gauge needles and syringes containing Dulbecco's Modified Eagle's Medium (DMEM; Gibco, USA). The resulting cell suspensions were plated in 100 mm cell culture dishes in DMEM (Gibco) supplemented with 10% foetal bovine serum, 100 U/ml penicillin, and 100 μg/ml streptomycin (all from Gibco). There were no osteogenic agents added to the culture medium. Cells were incubated in a humidified incubator at 37°C. The medium was replaced every three days. It has been reported that CD90 and CD146 are potential markers for BMMSCs.[17] We therefore used these two markers in the identification of BMMSCs in our experiments. After one week of culture, surface markers (CD90 and CD146) of BMMSCs were measured using flow cytometry. The cells were centrifuged, stained using fluorescently labelled primary antibodies (CD90, 1:100, Biolegend, USA; CD146, 1:100, R&D Systems, China) in the dark, and rinsed thrice with 1% bovine serum albumin. Finally, cell suspensions (500 μl) were added to a tube and examined using a Gallios flow cytometer (Beckman, USA). Data were analyzed using Kaluza software 2.1. P2–P3 BMMSCs were used in subsequent experiments.

Isolation and culture of rat macrophages. Primary macrophages were obtained by isolation of bone marrow progenitors from four-week-old male Sprague Dawley rats. The methods of macrophage isolation and identification have been reported in our previous work,[18] with 96% of the macrophages isolated expressing CD11b. Shortly after, rats were euthanized and the femora were aseptically collected. Bone marrow was flushed using 18-gauge needles and syringes containing DMEM (Gibco). The resulting cell suspensions were plated on 100 mm cell culture dishes containing DMEM medium supplemented with 30 ng/ml of macrophage colony-stimulating factor (PeproTech, USA). The media in the DT + 30 ng/ml of IL4 (DT + 30 IL4) and DT + 100 ng/ml of IL4 (DT + 100 IL4) groups were supplemented with 30 ng/ml and 100 ng/ml of IL4 (Peprotech), respectively, to mimic the biological transition from M1 to M2 phenotype. The medium was replaced every three days.

Immunofluorescence staining in vitro. After culturing BMMSCs (3 × 10^4) on the surface of the scaffolds in the 24-well plate for two days, nuclei and actin filaments were stained using 4',6-diamidino-2-phenylindole (DAPI; Beyotime, China) and phalloidin (YEASEN, China), respectively. Immunofluorescence (IF) staining was performed to measure expression levels of inducible nitric oxide synthase (iNOS; M1 marker) and CD206 (M2 marker). Following incubation on DT for three days, 3 × 10^4 macrophages were fixed in 4% paraformaldehyde, permeabilized using 0.1% Triton-X for 20 minutes, and incubated with primary antibodies from Abcam (USA) (Mouse anti-iNOS, 1:100, ab49999; rabbit anti-mannose receptor, 1:100, ab64693) and secondary antibodies purchased from Abbkine (USA) (DyLight 488, 1:500, goat anti-mouse immunoglobulin G (IgG); DyLight 594, 1:500, goat anti-rabbit IgG). Finally, the nuclei were stained blue with DAPI for 30 seconds. We also performed IF staining using osteocalcin (OCN) and vascular endothelial growth factor (VEGF) to evaluate the effect of scaffolds on the osteogenesis and angiogenic influence of BMMSCs. Following culture of BMMSCs on the samples for four days, the cells were fixed and incubated with primary (mouse anti-OCN, 1:100, ab13420; mouse anti-VEGFA, 1:100, ab1316; both from Abcam) and fluorescent antibodies.

Finally, cell adhesion morphology, iNOS, CD206, osteogenesis, and angiogenesis-related protein expression levels were measured using a laser scanning confocal microscope (Opera Phoenix; PerkinElmer, USA; image magnification for cell adhesion morphology was 63, image magnification for iNOS, CD206, osteogenesis, and angiogenesis-related protein expression was 20).

Single cell area. After staining the cells for cell adhesion, we used ImageJ software (National Institutes of Health, USA) to measure the area of a single cell. Three fields of view were repeated for each experimental group and control (DT only) group, and then were applied to statistical analysis.

Cell proliferation and apoptosis in vitro. Cytometry was employed to evaluate the proliferation of BMMSCs on DTs. Cells were seeded on DTs at 1.5 × 10^4 cells/ml in the 24-well plate. After culture for two, four, six, and eight days, the cells were rinsed twice with phosphate-buffered saline (PBS) to exclude the disruption of dead cells, and the remaining cells were trypsinized from the scaffolds and were counted using a blood cell counting chamber under a light microscope (DM4 B; Leica, Germany).

BMMSCs (3 × 10^5) were seeded on DTs in six-well plates, and cultured to confluence for 24 hours. The cells were collected using trypsin without ethylenediaminetetraacetic acid, and were washed twice with PBS. Subsequently, a fluorescein isothiocyanate annexin V apoptosis detection kit (YiShan Biotech, China) was used to identify the dead and apoptotic cells. According to the manufacturer's instructions, cells were resuspended in binding buffer and were mixed with annexin V-fluorescein isothiocyanate or propidium iodide at room temperature in the dark. Finally, a Gallios flow cytometer (Beckman,

Table I. Primers used in the reverse transcription polymerase chain reaction.

Accession number	Gene	Primer sequence (F, forward; R, reverse; 5'–3')	Product size, bp	Melting temperature/°C
NM_053650.2	ALP	F: ATGCTCAGGACAGGATCAAA	78	53.35
		R: CGGGACATAAGCGAGTTTCT		55.4
NM_053304.1	COL1	F: AGCTCGATACACAATGGCCT	209	55.4
		R: CCTATGACTTCTGCGTCTGG		57.45
NM_013414.1	OCN	F: CAGACAAGTCCCACACAGCA	85	57.45
		R: CCAGCAGAGTGAGCAGAGAG		59.5
NM_001278483.1	RUNX2	F: ATCATTCAGTGACACCACCA	141	53.35
		R: GTAGGGGCTAAAGGCAAAAG		55.4
NM_199489.4	CCR7	F: CATTTTCCAGGTGTGCTTCTGC	91	57.67
		R: CACCGACTCATACAGGGTGT		57.45
NM_001106123.2	CD206	F: GAGGACTGCGTGGTGATGAA	154	57.45
		R: CATGCCGTTTCCAGCCTTTC		57.45
NM_017178.2	BMP2	F: GCATGTTTGGCCTGAAGCAG	180	57.45
		R: CGATGGCTTCTTCGTGATGG		57.45
NM_031836.3	VEGF	F: AGAAAGCCCATGAAGTGGTGA	168	55.61
		R: CTTCATCATTGCAGCAGCCC		57.45
NM_031144.3	β actin	F: CCTCTATGACAACACAGT	155	50.34
		R: AGCCACCAATCCACACAG		54.9

ALP, alkaline phosphatase; BMP2, bone morphogenetic protein 2; CCR7, C-C motif chemokine receptor 7; COL1, type I collagen; RUNX2, runt-related transcription factor-2; VEGF, vascular endothelial growth factor.

Germany) was used to determine the percentage of dead and apoptotic cells in each group.

Quantitative reverse transcription polymerase chain reaction. BMMSCs (3×10^4) were seeded on DTs in 24-well plates and cultured to confluence for 48 hours. Then, total RNA was isolated from BMMSCs using RNA fast 200 (Fastagen, China). Reverse transcription of RNA was performed using reverse transcriptase ReverTra Ace (Toyobo, Japan). Quantitative reverse transcription polymerase chain reaction (RT-qPCR) was performed in thermal cyclers (95°C for 30 seconds, followed by 40 cycles at 95°C for five seconds, 55°C for ten seconds, and 72°C for 15 seconds) using specific primers (alkaline phosphatase (*ALP*), type I collagen (*COL1*), osteocalcin (*OCN*), runt-related transcription factor-2 (*RUNX2*)) and SYBR Green Realtime PCR Master Mix (Toyobo). The results were calculated by the comparative method of relative quantification ($2^{-\Delta\Delta CT}$ method). The primer details are shown in Table I with β actin as the housekeeping gene.

Alizarin red staining. BMMSCs (3×10^4) were cultured on DT implants in 24-well plates. First, the samples were fixed with 4% paraformaldehyde for ten minutes. Then, 0.2% alizarin red (Cyagen, China) was added to the wells and staining lasted 30 minutes. The final result was photographed, and solubilized by 10% acetum (Sinopharm Chemical Reagent Co, China) and 10% causticum solutum ammonium water solution (Sinopharm Chemical Reagent Co), respectively. Then, the absorbance at 405 nm was quantitatively measured.

Conditioned medium culture system in vitro. Macrophages (3×10^4) were cultured on the scaffolds in 24-well plates to evaluate the immunomodulatory osteogenic ability of materials. Following two days of incubation, the culture medium was collected and used to further culture BMMSCs. BMMSCs (3×10^4) were cultured on DT with completely conditioned medium in 24-well plates. RT-qPCR and IF staining were performed on day two after incubation of BMMSCs. Alizarin red staining was performed on day 14 after incubation.

Coculture system in vitro. BMMSCs (3×10^4) and macrophages (3×10^4) were mixed together and placed on the DT in 24-well plates. Fresh IL4 (30 ng/ml) was added daily in the culture medium on the first, third, fifth, and seventh days. The medium was replaced daily until day eight after incubation. At day eight after incubation, the ratio of M1/M2 was determined, and RT-qPCR was performed to measure time-dependent macrophage polarization. To quantify the ratio of M1/M2, we calculated the number of cells expressing iNOS or CD206 in each sample using the high content screening system (Opera Phoenix, PerkinElmer). RT-qPCR was performed as described. We changed the culture medium (without IL4) every three days from day eight onwards. RT-qPCR was performed to determine the time-dependent osteogenesis of BMMSCs (*ALP*, *COL1*, *OCN*, and *RUNX2*) at day 14.

DT implantation in vivo using a rat femur defect model. Five rats per group subcutaneously received 0.5 ml 10% chloral hydrate 30 minutes prior to surgery. The anaesthetized rats were positioned on the operating table in the lateral recumbent position with the right leg facing upwards. The operation site was shaved and aseptically prepared. We performed a lateral approach via a skin incision. We predrilled a hole (trabecular defect) with a diameter of approximately 2 mm (5 mm: critical defect size in a rat model)[19] along the longitudinal axis of the femur. Subsequently, samples were implanted into the femora. Incisions were sutured layer by layer. IL4 (30 ng) dissolved in 20 µl of saline was injected daily into the

surrounding tissue of the implanting field from days 3 to 7 after implantation in the DT + 30 IL4 group, as previously described.[11] After eight weeks, the rats were euthanized and their femora were removed for micro-CT and hard tissue section staining. No fractures were observed in any of the collected femora. The animal experimental study was approved by the ethics committee of the Qilu Hospital at Shandong University, China.

Micro-CT. All specimens were scanned and analyzed using a micro-CT system (SkyScan 2211; Bruker, Belgium). Scans were performed at 10 μm resolution in all three spatial dimensions, with 90 kV energy and 80 μA intensity. The region of interest was defined as a 2.6 mm circle around the implant. The lower and upper grey thresholds were 112 and 232, respectively. The length between lower and upper vertical positions (length of interest) was 5.22 mm. Morphometric parameters were determined at the 3D level and included new bone volume ratio (bone volume to total volume), trabecular thickness, and trabecular numbers using Dataviewer 1.5.6.2 (Bruker) and CTan 1.18.8.0 software (Bruker).

Hard tissue section staining. The femora extracted from the rats were fixed with ethyl alcohol for 72 hours and embedded in light curing resin (Technovit 7200VLC, Germany) for five days, and cut into sections (thickness: 30 μm). Subsequently, the hard tissue sections were stained with toluidine blue (Solarbio, China) following the manufacturer's instructions to evaluate the bone formation surrounding the implant. Finally, the slides were rinsed, covered, and observed under a light microscope (DM4 B; Leica; image magnification was 40 and 100).

DT implantation in vivo using a rat subcutaneous model. Five rats per group subcutaneously received 10% chloral hydrate 30 minutes prior to surgery. An incision was performed on the back of each rat, the sheets (10 mm × 10 mm × 1 mm) were placed subcutaneously below the incision, and the incision was sutured. IL4 (30 ng) dissolved in 20 μl of saline was injected daily into the surrounding tissue of the implanting field from days 3 to 7 after implantation in the DT + 30 IL4 group. After two weeks, the tissue around the sheet was removed to perform the RT-qPCR test as mentioned above. When separating the implant, the surface of the implant was wrapped with a relatively dense fibrous tissue close to the titanium sheet, with a thickness of about 0.1 mm.

Statistical analysis. Data were presented as means and standard deviations (SDs) from at least three independent experiments. Differences among groups were analyzed using one-way analysis of variance using SPSS Statistics version 23 (IBM, USA). A p-value < 0.01 was considered significant.

Results

Fabrication and characteristics of the DT. DT characteristics were tested using a scanning electron microscope and the BMMSCs were identified using CD90 and CD146 as labels on a flow cytometer. The micro-nanoscale morphology of the fabricated DT samples is illustrated in Figure 1. The scanning electron microscopy images showed non-melted Ti spherical powder particles with diameters of 50 μm on the surface of the DT. There were uneven pores between these non-melted spherical powder particles. Observation under high magnification revealed that the surface of the spherical powders was composed of Ti rods (with lengths of approximately 1 μm and diameters of approximately 100 nm) intertwined with one another. The results of energy-dispersive X-spectroscopy (EDS) showed that the main components of the DT were Ti and oxygen; other elements included aluminium, vanadium, calcium, and phosphorus. These elements were components of the raw materials and contributed to osteoinduction. The expression of antigens CD90 and CD146 on the surface of BMMSCs was measured using flow cytometry. We found that the cells were positive for CD90 (> 97%) and CD146 (> 97%) (Figure 1c).

In vitro biocompatibility of DT. BMMSCs were cultured on DT sheets for various time periods (two, four, six, and eight days) and were tested using a laser scanning confocal microscope, blood counting chamber, RT-qPCR, and flow cytometer to verify the biocompatibility of DT. As shown in Figure 2a, BMMSCs maintained polygonal shapes on the DT regardless of the concentration of IL4. However, the shape of BMMSCs on the DT was slightly flatter than on the others (Figure 2b). Nevertheless, there was no significant difference in the integrated density of phalloidin of BMMSCs in the DT, DT + 30 IL4, and DT + 100 IL4 groups.

We performed cytometry to determine the proliferation of BMMSCs in each group on days 2, 4, 6, and 8. As shown in Figure 2c, BMMSC proliferation on the DT + 30 IL4 group was slightly enhanced compared with those observed in the other groups. However, there was no significant difference between the groups. Moreover, there was no significant difference in the *ALP* mRNA expression between the DT, DT + 30 IL4, and DT + 100 IL4 groups (Figure 2d). BMMSCs were incubated for 24 hours to examine apoptosis using annexin V-propidium iodide flow cytometry. The number of dead cells in the DT + 30 IL4 group was similar to that recorded in the DT + 100 IL4 group, but lower than that observed on DT (Figure 2e). There was no significant difference among the DT, DT + 30 IL4, and DT + 100 IL4 groups.

Macrophage polarization on the DT. Following incubation (3×10^4) on DT for two days, the mRNA of macrophages was extracted and RT-qPCR was performed. After macrophages (3×10^4) were cultured on the surface of DT for two days, IF staining was performed, and the results were observed using a confocal microscope.

We selected some representative genes (*iNOS*, *CD206*, *VEGF*, bone morphogenetic protein 2 (*BMP2*)) of macrophages to confirm the role of IL4 in assisting DT to exert its immunomodulatory effects and to induce osteogenesis-related production of cytokines. We determined the fold-changes in the expression levels of these genes compared to those noted for DT using RT-qPCR

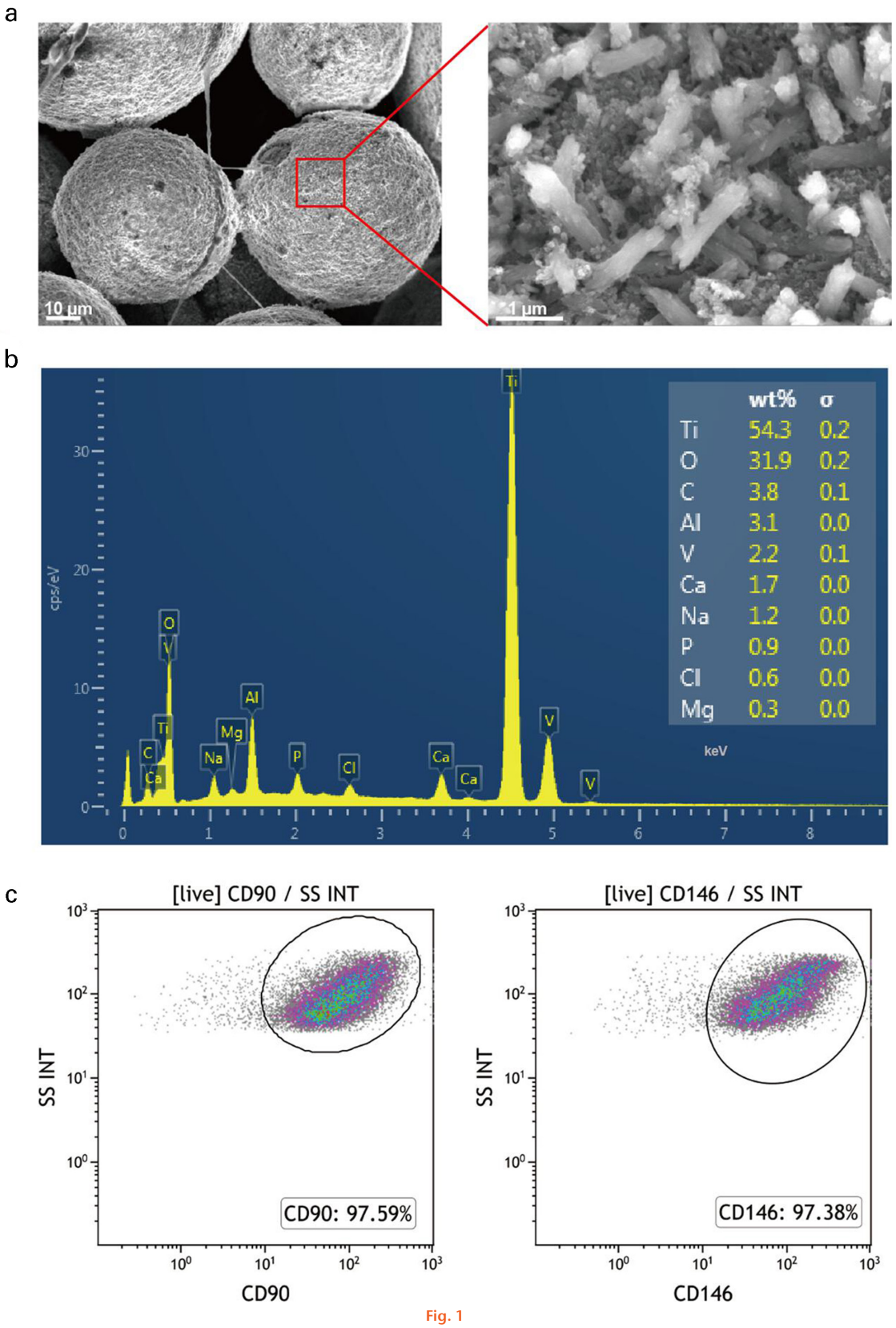

Fig. 1

Characterization of the 3D-printed titanium implant (DT). a) Surface morphologies of the DT by scanning electron microscopy (SEM). b) The energy dispersive X-spectroscope (EDS) spectra and relative content of each element. c) Surface markers of bone marrow mesenchymal stromal cells (BMMSCs) analyzed by flow cytometry. The cells were positive for CD90 and CD146.

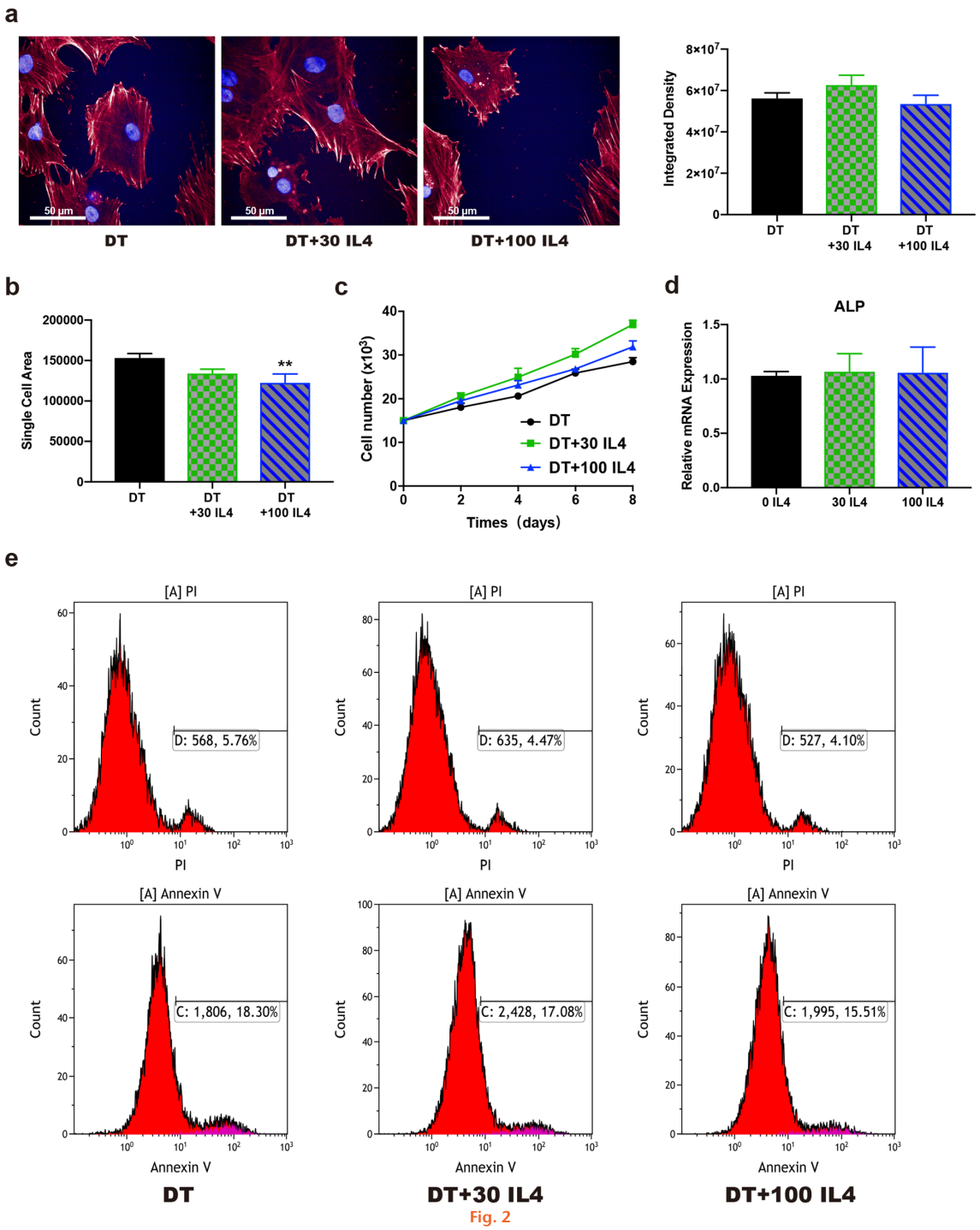

Fig. 2

Biocompatibility evaluation of the 3D printed titanium implant (DT) using bone marrow mesenchymal stromal cells (BMMSCs). a) Adhesion and morphology of BMMSCs in the DT, DT + 30 interleukin 4 (IL4), and DT + 100 IL4 groups by immunofluorescence staining; integrated density of phalloidin of BMMSCs in the DT, DT + 30 IL4, and DT + 100 IL4 groups. b) Area of a single cell in immunofluorescence staining images. **p < 0.01 compared with DT. c) Proliferation of BMMSCs cultured on the DT. d) Expression of alkaline phosphatase (*ALP*) mRNA of BMMSCs on the DT. e) Percentages of apoptotic BMMSCs cultured on the DT, evaluated by flow cytometry. DT + 30 IL4 and DT + 100 IL4 represent DT + 30 ng/ml of IL4 and DT + 100 ng/ml of IL4, respectively. mRNA, messenger RNA; PI, propidium iodide.

on day 2. As shown in Figure 3a, there were more M2 macrophages and higher expression of M2-related genes in the control group (macrophages seeded on the plate only) than in the DT group. These findings suggest that macrophage colony-stimulating factor tended to polarize macrophages towards M2 from the start. We also found significantly ($p < 0.01$) increased expression of *CD206*, but reduced expression of C-C motif chemokine receptor

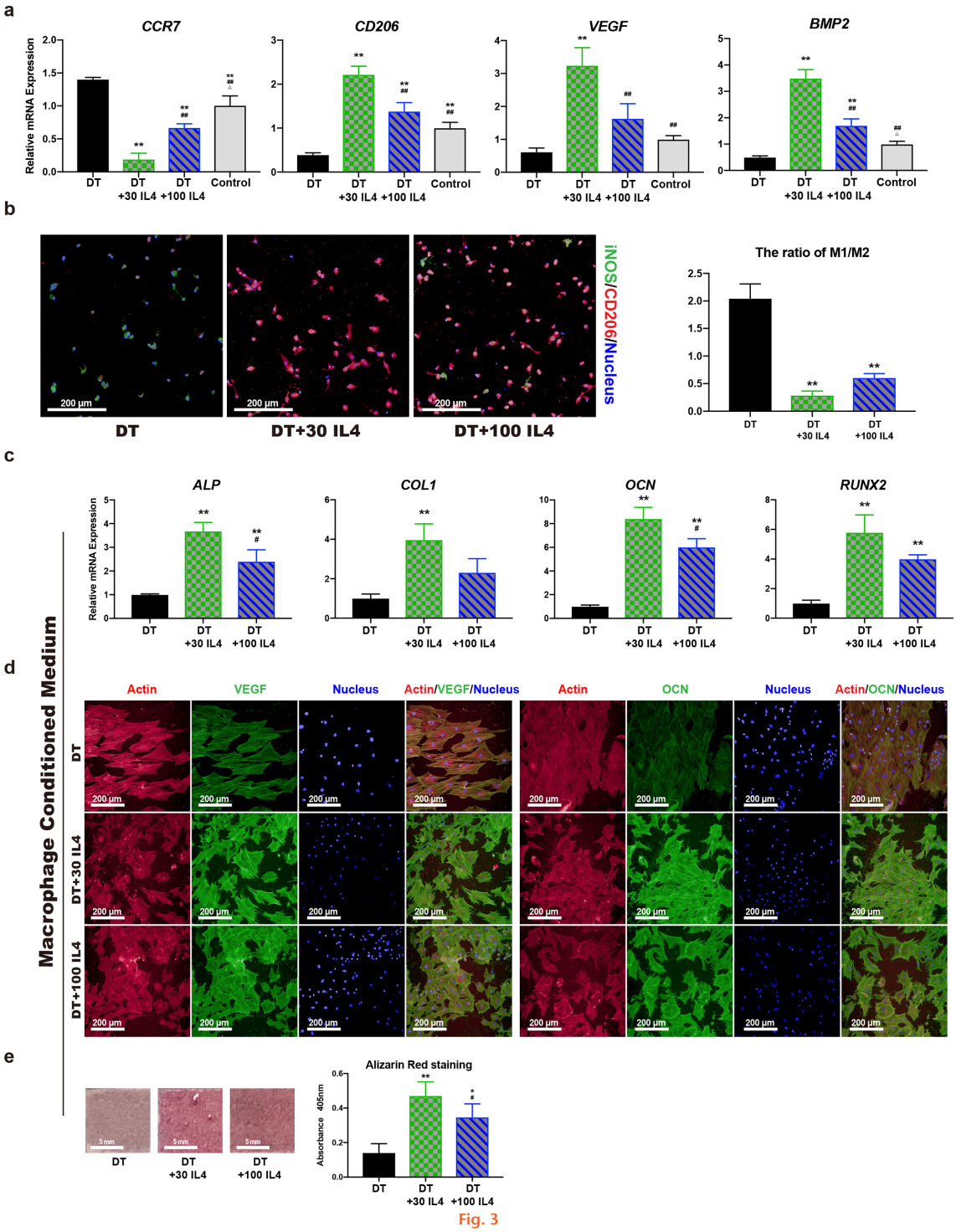

Fig. 3

3D-printed titanium implant (DT) with different doses of interleukin 4 (IL4) influences macrophage polarization and bone marrow mesenchymal stromal cell (BMMSC) osteogenesis. a) Expression of C-C motif chemokine receptor 7 (*CCR7*), *CD206*, vascular endothelial growth factor (*VEGF*), and bone morphogenetic protein 2 (*BMP2*) messenger RNA (mRNA) of macrophages in the DT, DT + 30 IL4, DT + 100 IL4, and control groups. b) Expression of inducible nitric oxide synthase (iNOS) and CD206 of macrophages and ratio of M1/M2 in the DT, DT + 30 IL4, and DT + 100 IL4 groups. Nucleus-DAPI, iNOS-DyLight 488, CD206-DyLight 594. c) Expression of osteogenesis (alkaline phosphatase (*ALP*), type I collagen (*COL1*), osteocalcin (*OCN*), and runt-related transcription factor-2 (*RUNX2*)) mRNA of BMMSCs in conditioned culture system. d) Immunofluorescent staining results of BMMSCs in conditioned culture system. Red denotes actin. Green denotes VEGF/OCN. Blue denotes 4′,6-diamidino-2-phenylindole (DAPI). e) Alizarin red staining of BMMSCs in the DT, DT + 30 IL4, and DT + 100 IL4 groups. $^{*}p < 0.05$ compared with DT. $^{**}p < 0.01$ compared with DT. $^{\#}p < 0.05$ compared with DT + 30 IL4. $^{\#\#}p < 0.01$ compared with DT + 30 IL4. DT + 30 IL4 and DT + 100 IL4 represent DT + 30 ng/ml of IL4 and DT + 100 ng/ml of IL4, respectively. M1, macrophage type 1; M2, macrophage type 2.

7 (*CCR7*) on DT + 30 IL4, suggesting that the ratio of M1/M2 had declined. Expression levels of *VEGF* (angiogenesis-related gene) and *BMP2* (osteogenesis-related gene) of macrophages were greater in the DT + 30 IL4 group than in the others, suggesting that DT + 30 IL4 tended to induce greater M2 production and was favourable to bone regeneration.

M1 marker (iNOS) and M2 marker (CD206) of macrophages cultured in different groups were measured using IF staining (Figure 3b). There were greater numbers of CD206-positive cells (red) and fewer iNOS-positive cells (green) in the DT + 30 IL4 group than in the DT and DT + 100 IL4 groups, respectively. This finding was consistent with the results of the RT-qPCR. The results of IF staining were similar to those of the ratio of M1/M2.

Osteogenesis differentiation of BMMSCs under the macrophage-conditioned culture system. We assessed the effects of macrophage polarization on the osteogenic differentiation of BMMSCs. BMMSCs were cultured in the conditioned medium obtained from the macrophages exposed to various concentrations of IL4. RT-qPCR and IF staining were performed on day 2 after incubation of BMMSCs. Alizarin red staining was performed to assess the osteogenic differentiation of BMMSCs on day 14 after incubation.

Upon exposure to various concentrations of IL4, *ALP* expression levels were elevated in BMMSCs (Figure 3c). Expression levels of osteogenic genes (*ALP, COL1, OCN, RUNX2*) in BMMSCs were greater after exposure to IL4. Expression levels of *ALP, COL1, OCN*, and *RUNX2* in BMMSCs in the DT + 100 IL4 group were slightly lower than those in the DT + 30 IL4 group; this was consistent with the results of *BMP2* expression (Figure 3a). To further evaluate the osteoimmunomodulatory effect on the samples, protein expression of VEGF (angiogenesis-related protein) and OCN (osteogenesis-related protein) was measured using IF staining. Figure 3d shows that the highest VEGF fluorescence (green) intensity was observed in the DT + 30 IL4 group, followed by the DT + 100 IL4 and DT groups. Consistent with the VEGF staining results, a similar trend was observed in OCN. Figure 3e shows that the highest degree of alizarin red expression was observed in the DT + 30 IL4 group, which was consistent with the results of osteogenic protein expression.

Time-dependent osteoimmunomodulation under the co-culture system. BMMSCs (3×10^4) and macrophages (3×10^4) were mixed together and placed on the DT in 24-well plates. Fresh IL4 (30 ng/ml) was added daily in the culture medium on the first, third, fifth, and seventh days in the various groups. The ratios of M1/M2 were determined and RT-qPCR was performed to evaluate time-dependent macrophage polarization on day 8 after incubation. After culturing for 14 days, alizarin red staining was performed to measure calcified nodule formation.

Figure 4b shows that the mean ratio of M1/M2 was increased from 0.33 (SD 0.12) in the Day 1 to 7 group to 2.44 (SD 0.35) in the Day 7 group. However, the ratio of M1/M2 in the Day 3 to 7 group was 1.29 (SD 0.27), indicating that the administration of IL4 from days 3 to 7 led to a balance between M1 and M2. Furthermore, macrophages in the Day 1 to 7 group showed elevated expression levels of *CD206*, *VEGF*, and *BMP2* mRNA, suggesting that the Day 1 to 7 group tended to induce greater production of M2 macrophages (Figure 4c). However, macrophages in the Day 7 group showed elevated *CCR7* mRNA expression levels, indicating that the Day 7 group tended to induce greater production of M1 macrophages. RT-qPCR was performed to measure time-dependent BMMSC osteogenesis (*ALP*, *COL1, OCN*, and *RUNX2*) at day 14. Expression levels of osteogenic genes (*ALP*, *COL1, OCN*, and *RUNX2*) and calcified nodule formation in BMMSCs were the highest in the Day 3 to 7 group. Expression levels of *ALP*, *COL1, OCN*, and *RUNX2* in cells in the Day 1 group were lower than those of the Day 3 and Day 5 groups. These results suggest that the lowest mean ratio of M1/M2 (0.33 (SD 0.12)) was not related to the best BMMSC osteogenesis.

DT repair in the rat femur defect model. Administration of IL4 from day 3 led to a balance of M1/M2 and the best osteogenesis of BMMSCs. For this reason, we performed in vivo experiments with daily administration of IL4 on days 3 to 7. Micro-CT and hard tissue section staining were used to assess new bone formation in the defect site and determine whether the delivery of IL4 would result in differences in bone formation, as shown in vitro. At eight weeks post-implantation, the femora were extracted and subjected to micro-CT analysis and hard tissue section staining.

Figure 5b illustrates the reconstructed images showing more bone formation in the DT + 30 IL4 group. Quantitative analysis (percentage of bone volume to total volume, trabecular numbers, trabecular thickness) revealed more osteogenesis in the DT + 30 IL4 group (Figure 5c). The bone adjacent to implants was stained positively with toluidine blue (Figure 5b). The DT + 30 IL4 group featured more bone growth surrounding the implants. Taken together, these findings suggest that the DT + 30 IL4 group was superior to DT in terms of bone regeneration in vivo.

Rat subcutaneous model. Sheets measuring 10 mm × 10 mm × 1 mm were placed subcutaneously below the skin of the back for two weeks. IL4 (30 ng) dissolved in 20 µl of saline was injected daily into the surrounding tissue of the implanting field at days 3 to 7 after implantation in the DT + 30 IL4 group. Finally, tissues around the sheets were removed to perform RT-qPCR. We selected some representative genes (*ALP*, *COL1*, *OCN*, *RUNX2*, *iNOS*, *CD206*, *VEGF*, and *BMP2*) to confirm the role of IL4 in assisting DT to exert immunomodulatory effects and to induce osteogenesis-related production of cytokines in vivo. We used RT-qPCR to determine the fold-changes in expression levels of these genes compared with those observed on DT.

As shown in Figure 5d, we found significantly greater expression levels of *ALP*, *COL1*, *OCN*, and *RUNX2* on DT + 30 IL4 in vivo, suggesting better osteogenesis ability of

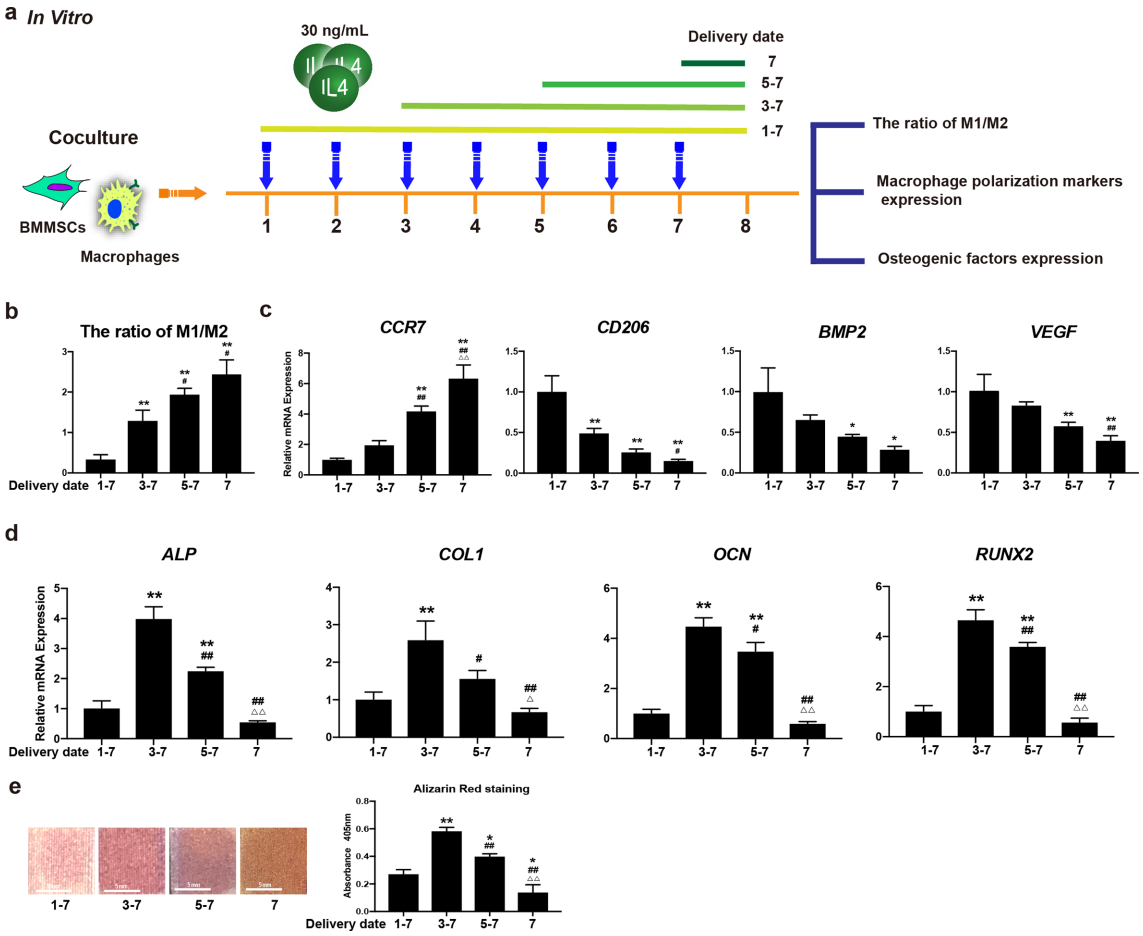

Fig. 4

3D-printed titanium implant (DT) with 30 ng/ml of interleukin 4 (IL4) at different timepoints influences macrophage polarization and bone marrow mesenchymal stromal cell (BMMSC) osteogenesis. a) Expression of osteogenic factors and macrophage phenotypes was assessed following IL4 delivery at different timepoints. b) The ratio of M1/M2 under the coculture system. c) Expression of C-C motif chemokine receptor 7 (*CCR7*), *CD206*, vascular endothelial growth factor (*VEGF*), and bone morphogenetic protein 2 (*BMP2*) messenger RNA (mRNA) of macrophages cocultured with BMMSCs on the DT. d) Expression of alkaline phosphatase (*ALP*), type I collagen (*COL1*), osteocalcin (*OCN*), and runt-related transcription factor-2 (*RUNX2*) mRNA of BMMSC cocultured with macrophages on the DT. e) Alizarin red staining of BMMSCs in the Day 1 to 7, 3 to 7, 5 to 7, and Day 7 groups. Differences among groups were analyzed with one-way analysis of variance. $^{*}p < 0.05$ compared with Day 1 to 7. $^{**}p < 0.01$ compared with day 1 to 7. $^{\#}p < 0.05$ compared with Day 3 to 7. $^{\#\#}p < 0.01$ compared with Day 3 to 7. $^{\triangle}p < 0.05$ compared with Day 5 to 7. $^{\triangle\triangle}p < 0.01$ compared with Day 5 to 7. M1, macrophage type 1; M2, macrophage type 2.

DT + 30 IL4. We also found significantly greater expression levels of *CD206*, but lower expression levels of *CCR7* on DT + 30 IL4, suggesting that the ratio of M1/M2 had declined. The expression of *VEGF* (angiogenesis-related gene) and *BMP2* (osteogenesis-related gene) in tissue was greater in the DT + 30 IL4 group than in the others. This suggests that DT + 30 IL4 group tended to induce greater production of M2 and was favourable to bone regeneration in vivo (Figure 5e).

Discussion

Several studies have found that an appropriate immunomicroenvironment is essential for acquiring ideal osseointegration of Ti implants.[10,20] Based on the personalized DT fabricated using EBM technology, we investigated the controllable polarization of macrophages regulated by DT + IL4. We found that DT with daily administration of 30 ng/ml of IL4 on days 3 to 7 achieved the best osteoimmunomodulation effect, which is favourable for the osseointegration of the implant.

Biocompatibility poses a significant challenge for manufacturers of medical devices, from the development of materials to market approval. All reactions of living cells in contact with materials determine the biocompatibility and safety of any device. Hence, the characterization of specific cell responses through adequate in vitro and in vivo experimentation is essential to guarantee controlled biocompatibility of a medical device.[21] The surface topography of the DT contains microspheres (Φ 50 μm) on the micro level and nanorods (1 μm × Φ 100 nm) on the nano level, which regulate cellular functions. Specifically, the microstructure is similar to the cell size and enhances the bone-implant anchorage, while the nanostructure is close to that of some cellular and extracellular matrix components. The results of the cytoskeleton, proliferation, and apoptosis analyses show that BMMSCs cultured on these

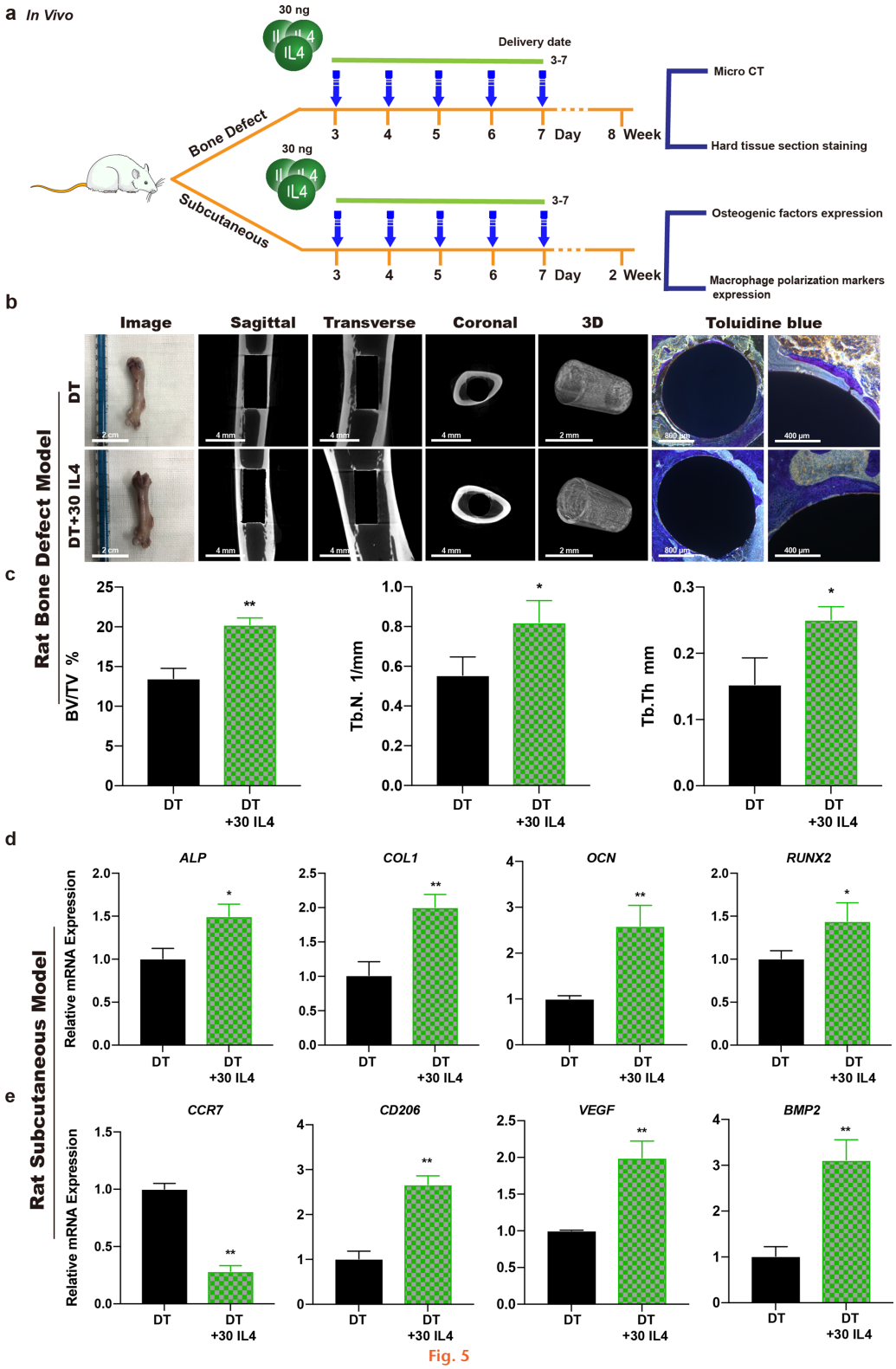

Fig. 5

Evaluation of osteogenic and inflammatory response using the femur defect and subcutaneous models. a) Experimental design for the in vivo evaluation of the immunomodulatory 3D-printed titanium implant (DT) femoral bone defect repair. b) Micro-CT images of femur defect model and toluidine blue staining of hard tissue sections. c) Quantitative analysis of micro-CT data: bone volume to total volume percentage (BV/TV%), trabecular numbers (Tb.N), and trabecular thickness (Tb.Th), respectively. d) Expression of alkaline phosphatase (*ALP*), type I collagen (*COL1*), osteocalcin (*OCN*), and runt-related transcription factor-2 (*RUNX2*) messenger RNA (mRNA) in tissue around samples. e) Expression of C-C motif chemokine receptor 7 (*CCR7*), *CD206*, vascular endothelial growth factor (*VEGF*), and bone morphogenetic protein 2 (*BMP2*) mRNA in tissues around samples. Differences among groups were analyzed with one-way analysis of variance. $^{*}p < 0.05$ compared with DT. $^{**}p < 0.01$ compared with DT.

samples generally demonstrated good cell viability and proliferation. The cell adhesion and basic cell function of BMMSCs were not affected by treatment with IL4. These results laid a foundation for subsequent studies of osteogenesis and inflammatory modulation in vitro and in vivo without the influence of biocompatibility.

Inflammatory modulation plays a crucial role in bone tissue engineering, which has been studied extensively.[22,23] A substantial body of evidence suggests that immune cells interact with the skeletal system and play important roles in post-healing processes.[24] At 24 hours following bone injury, the immune response reaches its peak, and is characterized by the release of inflammatory cytokines, contributing to early angiogenesis. The aim of the present study was to fabricate and optimize a novel surface modification for Ti implants, which promotes osteogenesis, inhibits inflammation, and can be used to treat bone defects. However, DT induces M1 polarization due to its rough surface (Figures 3a and 3b). It has been reported that M1 macrophages can clear debris and foreign bodies,[9] and a 72- to 96-hour proinflammatory environment (M1-related) is critical for optimal matrix mineralization.[25] Moreover, continuous presence of M1 macrophages provokes an inflammatory response and osteolysis, both of which can lead to an adverse impact on osteogenesis.[26] In fact, the M1 and M2 phenotypes are two extremes of the continuum of macrophage function. M2 macrophages play important roles in wound healing and angiogenesis in the late stages of inflammation.[27] It has been previously shown that M1 macrophages initiate angiogenesis while M2 macrophages promote vessel maturation; thus, it has been reasoned that scaffolds that promote sequential M1 and M2 polarization of infiltrating macrophages should result in enhanced angiogenesis and healing.[28] The precise immunomodulation of the M1 to M2 transition is important for the enhanced osteogenesis of BMMSCs.

IL4 (an agonist of M2 polarization) was used to switch macrophages to M2 polarization and to promote osteogenesis in vitro. Enhanced expression levels of *VEGF* and *BMP2* were associated with M2 polarization (Figure 3). IL4 promotes macrophage M2 polarization via the JNK signalling pathway.[29] We also found that M2 macrophages play important roles in the granulation tissue formation and matrix remodelling phases.[30] The best defect healing outcome, with complete defect bridging at 12 weeks, occurred in the 10 ng group.[11] This was followed by the 50 ng and 0 ng groups, with partial defect bridging; the 100 ng group exhibited nonunion healing in the large cranial bone defect model.[11] In the present study, the conditioned medium from the DT + 30 IL4 and DT + 100 IL4 groups enhanced osteogenesis and the angiogenic potential of BMMSCs, demonstrating that IL4 mediated osteogenesis and angiogenesis. As shown in Figure 3c, RT-qPCR indicated that the BMMSCs in the DT + 30 IL4 group tended to have higher expression levels of osteogenic genes such as *ALP*, *COL1*, *OCN*, and *RUNX2*, all of which are necessary for osteogenesis.[31,32] The immunofluorescence results showed similar trends, suggesting that macrophages in the DT + 30 IL4 group tend to secrete more pro-osteogenic and proangiogenic cytokines, thereby promoting BMMSC osteogenesis and angiogenic potential. This is consistent with the results shown in Figure 3a, demonstrating that macrophages in the DT + 30 IL4 group showed enhanced expression levels of *BMP2* and *VEGF* mRNA. Daily administration of 30 ng/ml of IL4 on days 3 to 7 generated a balanced M1/M2 ratio and led to better osteogenesis in the coculture system (Figure 4). Collectively, these in vitro data demonstrated that DT+ IL4 (M1- and M2-coordinated) improves osteogenesis and angiogenic potential more than DT alone (M1-related).

The in vivo environment is extremely complex; in addition to BMMSCs and macrophages, it is rich in various other cells and cytokines. Most studied biomaterials should be used in vivo, in which the evaluation of restorative effects are more similar to the actual situation. M1 macrophages clear debris and produce optimal matrix mineralization; interruption in the early fracture healing process is thought to have an adverse impact on the regeneration cascade. The M1-mediated proinflammatory process is followed by a post-healing period, seven to ten days after the injury, during which time bone formation is initiated.[33,34] The expression of inflammatory cytokines is lower during the post-healing period, which is driven by BMP2 and other osteogenic factors.[35]

Evidence is emerging to support a broader role of M1 macrophages in inducing the downstream inflammatory cascade.[36] The timing of the local delivery of IL4 was delayed to three days post implantation, i.e. the time during normal bone healing when the levels of inflammatory cytokines begin to decline.[10,33] It has been shown that sustained delivery of anti-inflammatory factors is beneficial for tissue repair.[37] Hence, daily injection of IL4 was performed on days 3 to 7. The combination of scaffold and biological response modifier (IL4) capable of polarizing the macrophage phenotype has been considered as a potential strategy for enhancing constructive bone formation.[11] Interestingly, the performances of osteogenesis in vivo and under the conditioned culture system in vitro were remarkably similar. The results on IL4-assisted DT in the femur of rats also supported this notion; the findings suggest that DT + 30 IL4 (daily administration on days 3 to 7) had better immune modulatory ability and bone regenerative properties.

Previous studies reported that IL4 promoted M2 macrophage polarization in several materials.[11,15,16] The innovation of our study lies, first, in the difference in material modification; we used 3D printing technology, which is more conducive to clinical use, especially in cases of acetabular fracture. Different morphologies have different impact mechanisms and effects on immune cells and osteoblasts; therefore, the specificity of the material is explained based on the morphological characteristics. Further investigation of osteoimmunomodulation is necessary. Second, we evaluated the dosage and timing

of IL4 administration. It was reported that cytokines also played anti-inflammatory and pro-osteogenic roles.[38]

In the present study, increased expression levels of *ALP*, *COL1*, *OCN*, and *RUNX2* were observed in the DT + 100 IL4 group. Although recent studies reported that M2 macrophage polarization was beneficial to bone formation,[39] excessive M2 macrophage polarization has also been shown to induce profibrotic effects and promote macrophage fusion into foreign body giant cells in vitro and in vivo.[40,41] These effects may lead to reduced osteogenesis. Further understanding of the underlying mechanism is required to provide insight into new osteoimmunomodulatory materials. Nevertheless, the present data offer compelling evidence that DT + 30 IL4 (daily administration on days 3 to 7) is intrinsically anti-inflammatory and pro-osteogenic (Figures 4 and 5). The significance of this study lies in the fact that accurate adjustment of the bone immune microenvironment plays an important role after 3D-printed prostheses are implanted. In summary, our data suggest that DT + 30 IL4 is an osteoimmunomodulatory biomaterial. Further investigations are warranted to fully illustrate the mechanisms of IL4 in M2 macrophage-mediated immune responses.

Supplementary material

ARRIVE checklist

References

1. **Chen Z**, **Visalakshan RM**, **Guo J**, **et al**. Plasma deposited poly-oxazoline nanotextured surfaces dictate osteoimmunomodulation towards ameliorative osteogenesis. *Acta Biomater*. 2019;96:568–581.
2. **Li B**, **Ma J**, **Wang D**, **et al**. Self-adjusting antibacterial properties of Ag-incorporated nanotubes on micro-nanostructured Ti surfaces. *Biomater Sci*. 2019;7(10):4075–4087.
3. **Sibisi PN**, **Popoola API**, **Arthur NKK**, **Pityana SL**. Review on direct metal laser deposition manufacturing technology for the TI-6AL-4V alloy. *Int J Adv Manuf Technol*. 2020;107(3–4):1163–1178.
4. **Li X**, **Huang Q**, **Elkhooly TA**, **et al**. Effects of titanium surface roughness on the mediation of osteogenesis via modulating the immune response of macrophages. *Biomed Mater*. 2018;13(4):045013.
5. **Hotchkiss KM**, **Reddy GB**, **Hyzy SL**, **Schwartz Z**, **Boyan BD**, **Olivares-Navarrete R**. Titanium surface characteristics, including topography and wettability, alter macrophage activation. *Acta Biomater*. 2016;31:425–434.
6. **Franz S**, **Rammelt S**, **Scharnweber D**, **Simon JC**. Immune responses to implants - a review of the implications for the design of immunomodulatory biomaterials. *Biomaterials*. 2011;32(28):6692–6709.
7. **Wang J**, **Meng F**, **Song W**, **et al**. Nanostructured titanium regulates osseointegration via influencing macrophage polarization in the osteogenic environment. *Int J Nanomedicine*. 2018;13:4029–4043.
8. **Marsell R**, **Einhorn TA**. The biology of fracture healing. *Injury*. 2011;42(6):551–555.
9. **Julier Z**, **Park AJ**, **Briquez PS**, **Martino MM**. Promoting tissue regeneration by modulating the immune system. *Acta Biomater*. 2017;53:13–28.
10. **Loi F**, **Cordova LA**, **Zhang R**, **et al**. The effects of immunomodulation by macrophage subsets on osteogenesis in vitro. *Stem Cell Res Ther*. 2016;7:15.
11. **Zheng ZW**, **Chen YH**, **Wu DY**, **et al**. Development of an Accurate and Proactive Immunomodulatory Strategy to Improve Bone Substitute Material-Mediated Osteogenesis and Angiogenesis. *Theranostics*. 2018;8(19):5482–5500.
12. **Zhang H**, **Wu X**, **Wang G**, **et al**. Macrophage polarization, inflammatory signaling, and NF-κB activation in response to chemically modified titanium surfaces. *Colloids Surf B Biointerfaces*. 2018;166:269–276.
13. **Xu WC**, **Dong X**, **Ding JL**, **et al**. Nanotubular TiO_2 regulates macrophage M_2 polarization and increases macrophage secretion of VEGF to accelerate endothelialization via the ERK1/$_2$ and PI3K/AKT pathways. *Int J Nanomedicine*. 2019;14:441–455.
14. **Yang CL**, **Sun YH**, **Yu WH**, **Yin XZ**, **Weng J**, **Feng B**. Modulation of macrophage phenotype through controlled release of interleukin-4 from gelatine coatings on titanium surfaces. *Eur Cell Mater*. 2018;36:15–29.
15. **Kohno Y**, **Lin T**, **Pajarinen J**, **et al**. Treating titanium particle-induced inflammation with genetically modified NF-κB Sensing IL-4 secreting or preconditioned mesenchymal stem cells in vitro. *ACS Biomater Sci Eng*. 2019;5(6):3032–3038.
16. **Wang Y**, **Qi H**, **Miron RJ**, **Zhang Y**. Modulating macrophage polarization on titanium implant surface by poly(dopamine)-assisted immobilization of IL4. *Clin Implant Dent Relat Res*. 2019;21(5):977–986.
17. **Li S**, **Guo YW**, **Wang ZY**, **Ning ZR**, **Fang DJ**. [The isolation and identification of bone marrow mesenchymal stem cells derived from rabbit mandible]. *Shanghai Kou Qiang Yi Xue*. 2013;22(1):19–24. (Article in Chinese)
18. **Zhao D-W**, **Liu C**, **Zuo K-Q**, **et al**. Strontium-zinc phosphate chemical conversion coating improves the osseointegration of titanium implants by regulating macrophage polarization. *Chemical Engineering Journal*. 2021;408:127362.
19. **Poser L**, **Matthys R**, **Schawalder P**, **Pearce S**, **Alini M**, **Zeiter S**. A standardized critical size defect model in normal and osteoporotic rats to evaluate bone tissue engineered constructs. *Biomed Res Int*. 2014;2014:348635.
20. **Brown BN**, **Badylak SF**. Expanded applications, shifting paradigms and an improved understanding of host-biomaterial interactions. *Acta Biomater*. 2013;9(2):4948–4955.
21. **Bernard M**, **Jubeli E**, **Pungente MD**, **Yagoubi N**. Biocompatibility of polymer-based biomaterials and medical devices - regulations, in vitro screening and risk-management. *Biomater Sci*. 2018;6(8):2025–2053.
22. **Xu X**, **Li Y**, **Wang L**, **et al**. Triple-functional polyetheretherketone surface with enhanced bacteriostasis and anti-inflammatory and osseointegrative properties for implant application. *Biomaterials*. 2019;212:98–114.
23. **Shen X**, **Zhang Y**, **Ma P**, **et al**. Fabrication of magnesium/zinc-metal organic framework on titanium implants to inhibit bacterial infection and promote bone regeneration. *Biomaterials*. 2019;212:1–16.
24. **Martino MM**, **Maruyama K**, **Kuhn GA**, **et al**. Inhibition of IL-1R1/MyD88 signalling promotes mesenchymal stem cell-driven tissue regeneration. *Nat Commun*. 2016;7:11051.
25. **Nathan K**, **Lu LY**, **Lin T**, **et al**. Precise immunomodulation of the M1 to M2 macrophage transition enhances mesenchymal stem cell osteogenesis and differs by sex. *Bone Joint Res*. 2019;8(10):481–488.
26. **Eger M**, **Hiram-Bab S**, **Liron T**, **et al**. Mechanism and prevention of titanium particle-induced inflammation and osteolysis. *Front Immunol*. 2018;9:2963.
27. **Gordon S**. Alternative activation of macrophages. *Nat Rev Immunol*. 2003;3(1):23–35.
28. **Spiller KL**, **Nassiri S**, **Witherel CE**, **et al**. Sequential delivery of immunomodulatory cytokines to facilitate the M1-to-M2 transition of macrophages and enhance vascularization of bone scaffolds. *Biomaterials*. 2015;37:194–207.
29. **Hao J**, **Hu Y**, **Li Y**, **Zhou Q**, **Lv X**. Involvement of JNK signaling in IL4-induced M2 macrophage polarization. *Exp Cell Res*. 2017;357(2):155–162.
30. **Gordon S**, **Martinez FO**. Alternative activation of macrophages: mechanism and functions. *Immunity*. 2010;32(5):593–604.
31. **Shi M**, **Chen Z**, **Farnaghi S**, **et al**. Copper-doped mesoporous silica nanospheres, a promising immunomodulatory agent for inducing osteogenesis. *Acta Biomater*. 2016;30:334–344.
32. **Wu C**, **Zhou Y**, **Xu M**, **et al**. Copper-Containing mesoporous bioactive glass scaffolds with multifunctional properties of angiogenesis capacity, osteostimulation and antibacterial activity. *Biomaterials*. 2013;34(2):422–433.
33. **Dimitriou R**, **Tsiridis E**, **Giannoudis PV**. Current concepts of molecular aspects of bone healing. *Injury*. 2005;36(12):1392–1404.
34. **Kon T**, **Cho TJ**, **Aizawa T**, **et al**. Expression of osteoprotegerin, receptor activator of NF-kappaB ligand (osteoprotegerin ligand) and related proinflammatory cytokines during fracture healing. *J Bone Miner Res*. 2001;16(6):1004–1014.
35. **Cheng NC**, **Estes BT**, **Awad HA**, **Guilak F**. Chondrogenic differentiation of adipose-derived adult stem cells by a porous scaffold derived from native articular cartilage extracellular matrix. *Tissue Eng Part A*. 2009;15(2):231–241.
36. **Bank RA**, **Zandstra J**, **Room H**, **Petersen AH**, **van Putten SM**. Biomaterial Encapsulation Is Enhanced in the Early Stages of the Foreign Body Reaction During Conditional Macrophage Depletion in Transgenic Macrophage Fas-Induced Apoptosis Mice. *Tissue Eng Part A*. 2017;23(19-20):1078–1087.
37. **Hachim D**, **LoPresti ST**, **Yates CC**, **Brown BN**. Shifts in macrophage phenotype at the biomaterial interface via IL-4 eluting coatings are associated with improved implant integration. *Biomaterials*. 2017;112:95–107.
38. **Mahon OR**, **Browe DC**, **Gonzalez-Fernandez T**, **et al**. Nano-particle mediated M2 macrophage polarization enhances bone formation and MSC osteogenesis in an IL-10 dependent manner. *Biomaterials*. 2020;239:119833.

39. **Hu Z**, **Ma C**, **Rong X**, **Zou S**, **Liu X**. Immunomodulatory ECM-like microspheres for accelerated bone regeneration in diabetes mellitus. *ACS Appl Mater Interfaces*. 2018;10(3):2377–2390.
40. **Moore LB**, **Sawyer AJ**, **Saucier-Sawyer J**, **Saltzman WM**, **Kyriakides TR**. Nanoparticle delivery of miR-223 to attenuate macrophage fusion. *Biomaterials*. 2016;89:127–135.
41. **Kao WJ**, **McNally AK**, **Hiltner A**, **Anderson JM**. Role for interleukin-4 in foreign-body giant cell formation on a poly(etherurethane urea) in vivo. *J Biomed Mater Res*. 1995;29(10):1267–1275.

Author information:

- D-W. Zhao, MSc, PhD Student, Department of Orthopedics, Qilu Hospital of Shandong University, Jinan, China; Cheeloo College of Medicine, Shandong University, Jinan, China; Institute of Stomatology, Shandong University, Jinan, Shandong, China.
- B. Ren, MSc, PhD Student, Key Laboratory of High Efficiency and Clean Manufacturing, School of Mechanical Engineering, Shandong University, Jinan, China; National Demonstration Center for Experimental Mechanical Engineering Education, School of Mechanical Engineering, Shandong University, Jinan, China; Department of Mechanical and Aerospace Engineering, University of Florida, Gainesville, Florida, USA.
- H-W. Wang, MSc, PhD Student
- X. Zhang, MD, Student
- M-Z. Yu, MD, Student
- Y. Wan, PhD, Professor
  Key Laboratory of High Efficiency and Clean Manufacturing, School of Mechanical Engineering, Shandong University, Jinan, China; National Demonstration Center for Experimental Mechanical Engineering Education, School of Mechanical Engineering, Shandong University, Jinan, China.
- L. Cheng, PhD, Professor, Chief Physician, Department of Orthopedics, Qilu Hospital of Shandong University, Jinan, China.
- Y-H. Sang, PhD, Professor, State Key Laboratory of Crystal Materials, Shandong University, Jinan, Shandong, China.
- S-S. Cao, PhD, Surgeon
- F. M. Thieringer, PhD, Professor
  Medical Additive Manufacturing Research Group, Department of Biomedical Engineering, University of Basel, Basel, Switzerland; Department of Oral and Cranio-Maxillofacial Surgery, University Hospital Basel, Basel, Switzerland.
- D. Zhang, PhD, Professor, Associate Chief Physician
- C. Liu, PhD, Professor, Associate Chief Physician
  Institute of Stomatology, Shandong University, Jinan, Shandong, China; Department of Oral and Maxillofacial Surgery, Qilu Hospital of Shandong University, Jinan, China.

Author contributions:

- D-W. Zhao: Designed the study, Acquired the data, Helped to draft the article.
- B. Ren: Analyzed and interpreted the data, Helped to draft the article.
- H-W. Wang: Analyzed and interpreted the data, Drafted the article, Approved the final version to be submitted for publication.
- X. Zhang: Analyzed and interpreted the data, Helped to draft the article.
- M-Z. Yu: Analyzed and interpreted the data, Helped to draft the article.
- L. Cheng: Designed the study, Helped to draft the article.
- Y-H. Sang: Designed the study, Helped to draft the article.
- S-S. Cao: Acquired the data, Helped to draft the article.
- F. M. Thieringer: Acquired the data, Helped to draft the article.
- D. Zhang: Designed the study, Helped to draft the article.
- Y. Wan: Designed the study, Helped to draft the article.
- C. Liu: Designed the study, Helped to draft the article.

Funding statement:

- This work was supported by the Shandong Provincial Natural Science Foundation (Grant nos. BS2015SW028 and 2017G006010), Clinical Science and Technology Innovation Plan of Jinan (Grant no. 201805052), Interdisciplinary open project of Advanced Medical Research Institute of Shandong University (Grant no. 22480082038410) and Bilateral research collaboration with Asia 2017-2020 (Swiss) (Grant no. IPG 01-112019).